



Structural Characterization and Optical Properties of BiFeO₃ Nanoparticles Synthesized by Propylene Glycol-Gel Route

MADHU VERMA^{1,✉}, SWETANGI SUMAN^{1,✉}, PREM MOHAN MISHRA^{1,✉} and SIMANT KUMAR SRIVASTAV^{1,2,*}

¹University Department of Chemistry, L.N. Mithila University, Darbhanga-846008, India

²Department of Chemistry, University of Allahabad, Prayagraj-211002, India

*Corresponding author: E-mail: sksrivastava@allduniv.ac.in; simant.iitk@gmail.com

Received: 27 August 2024;

Accepted: 16 October 2024;

Published online: 30 October 2024;

AJC-21796

This work focuses on the synthesis of phase-pure rhombohedral (*R3c*) nanocrystalline BiFeO₃. The BiFeO₃ nanoparticles were synthesized using the sol-gel method with propylene glycol as the complexing agent. The formation mechanism was investigated through thermal analysis and IR spectroscopy. The phase purity, crystal structure and nanocrystalline properties were studied using X-ray diffraction (XRD), Raman spectroscopy and transmission electron microscopy (TEM). The elemental composition and bonding states were analyzed with X-ray photoelectron spectroscopy (XPS). The XRD and Raman spectra confirmed the formation of pure and well-crystallized BiFeO₃ nanoparticles at 400 °C. The optical band gap, determined by UV-visible spectroscopy, was found to be 2.08 eV, indicating that the synthesized BiFeO₃ nanoparticles could be an effective photocatalyst in the visible light region.

Keywords: Bismuth ferrite, Propylene glycol, Sol-gel method, Phase stability, Band gap.

INTRODUCTION

Both the air and the water are contaminated by the ongoing rapid industrialization. The wastewater from textile, leather, cosmetic and paper industries contains organic dye molecules. The organic dye molecules are diluting and mixing to the water even in low concentration, which results in substantial water contamination. The dye-contaminated waste water is very harmful for water in habitated plants and organisms and also harmful for whole ecosphere [1,2]. Therefore, there is an urgent need to invent technique to decontaminate dye wastewater to make it useful for human beings. Several approaches have been used to overcome this issue [3-5]. In the field of solar radiation transformation and atmospheric purification, photocatalysis of semiconductor based nanomaterial have emerged as one of the most promising “green and safe” purification technologies in recent decades [6-10]. Photocatalysis, in which solar source available in abundance and the free of cost, is one of the most favourable and energy efficient methods at low cost to convert solar power into chemical energy in semiconductors. Although semiconductor materials like TiO₂, ZnO and CdS are extensively studied as photocatalyst, their large band gaps have resulted in limited photocatalytic activity under visible light [6-12].

Recent years have seen a significant increase in interest in bismuth based semiconductors because of their unusual structure and distinctive physical characteristics [13-15]. The intrinsic multiferroic property of BFO, along with its narrow band gap, high chemical stability and non-toxicity, has allowed it to become a prominent material in the field of semiconductor photocatalysis. Its photocatalytic properties under visible light have also been extensively studied in recent years [14,16-19]. The rhombohedral distorted perovskite structure of bismuth ferrite, BiFeO₃ (BFO), with a space group of *R3c*, demonstrates simultaneous ferroelectric ($T_C \sim 830$ °C) and antiferromagnetic ($T_N \sim 370$ °C) ordering [20-22]. Despite its potential in photocatalysis, the synthesis single-phase bismuth ferrite nanoparticles area very difficult task caused by its short temperature stability range [23,24]. To synthesize BFO nanoparticles various approaches have been adopted [25,26]. These processes are complicated or require for high temperatures during the calcination process, which causes bismuth to be lost by volatilization and gives the BFO phase in addition to impurity phases such as Bi₂Fe₄O₉, Bi₃₆Fe₂₄O₅₇, Bi₂O₃ and Fe₂O₃, among others [24,25]. Among them, the sol-gel approach is especially interesting since, in contrast to other approaches, it guarantees accurate

control over the composition of the precursor, tunability and ease of processing through efficient mixing and dispersion of cations in solution.

By using sol-gel method nanocrystalline BFO has been synthesized with various complexing agents, for example, polyvinyl alcohol, ethylene glycol and glycerol monomer, which have only -OH group but not COOH group are used in synthesis of BFO and these all can synthesized pure BFO easily [27-29]. By using tartaric acid (having two OH and two COOH group) and malic acid (having one OH groups and two COOH groups) single phase BFO can also be synthesized [30]. However, single phase BFO cannot be synthesized by utilizing succinic acid and malonic acid, which contains two COOH groups but no OH groups [31]. Citric acid contains one OH group and three COOH groups. Thus, for synthesis phase pure BFO the citrate method cannot be used [32]. When ethylene glycol is used as polymerizing agent, citrate precursor can be used to obtain pure BFO but malonic acid, succinic acid and EDTA (with four COOH, no OH) precursors do not act similarly [31,33,34]. Consequently, it is significant that the OH group facilitates BFO formation while the COOH group discourages formation. Thus, the synthesis of pure BFO with a new complexing agent having more OH groups and less COOH groups is possible [35].

In present work, a simple sol-gel method is applied with complexing agent propylene glycol (two OH groups and no COOH group) to synthesize pure BFO nanoparticles calcined at 400 °C. As synthesized pure BFO nanoparticles were characterized for their crystal structure, size, morphology and band gap.

EXPERIMENTAL

Analytical grade chemicals were utilized without additional purification *viz.* propylene glycol (Thomas Baker, India), nitric acid (Merck, Germany), ferric nitrate nonahydrate and bismuth nitrate pentahydrate (Sigma-Aldrich, USA). Precursor solution preparation involves the mixing $\text{Bi}(\text{NO}_3)_3 \cdot 5\text{H}_2\text{O}$ (dissolved in diluted nitric acid) and $\text{Fe}(\text{NO}_3)_3 \cdot 9\text{H}_2\text{O}$ (dissolved in distilled water) solutions in the appropriate mole ratio. Under continuous stirring, complexing agent was mixed to the aforementioned solution in a 1:1 mol ratio with respect to metal nitrates. After that, the mixture was heated to about 100 °C while being continuously stirred until all of the liquid evaporated. The resulting fluffy brown powder was calcined in muffle furnace under ambient environment at 400 °C for 2 h and yields well-crystallized BFO nanoparticles. The bismuth solution has relatively low calcination temperature and this minimizes the possibility of loss of volatile bismuth.

Characterization: Differential scanning calorimetry (DSC) and thermogravimetric analysis (TGA) of the precursor were

conducted using a Mettler Toledo Star System TGA/DSC instrument, with a heating rate of 10 °C/min under ambient conditions up to 850 °C. A Bruker Vertex-70 Fourier transform infrared (FT-IR) spectrometer was employed to determine the chemical connectivity of the BFO precursor and powder. The X-ray diffraction (XRD) analysis was performed using an X'Pert Pro (PANalytical, Netherlands) operating at 40 kV and 40 mA with Ni-filtered $\text{CuK}\alpha$ radiation ($\lambda = 0.15406$ nm) to assess the phase purity and crystal structure of the calcined powders. The morphology and crystallinity of the sample were examined with a transmission electron microscope (TEM) (FEI Technai G2 U-Twin) at an accelerating voltage of 200 kV. The X-ray photoelectron spectroscopy (XPS) data were obtained using a commercial electron energy analyzer (Specs GmbH, Germany) equipped with five channeltrons and an Al $\text{K}\alpha$ laboratory X-ray source operating at 100 watts, under a base pressure of 3×10^{-10} mbar. The Raman measurements in the 100-800 cm^{-1} range at room temperature were carried out with a Raman spectrometer (WITec, GmbH, Germany) using an excitation wavelength of 514.5 nm. The UV-visible absorption spectra of the BFO nanoparticles were recorded with a Varian Cary-100 UV-visible spectrophotometer.

RESULTS AND DISCUSSION

Thermal studies: The thermal decomposition stages of the BFO precursor powder are revealed by the TGA/DSC/DTG curves as displayed in Fig. 1. The breakdown of nitrate, carbonization and volatilization of propylene glycol and the dehydration of precursor may all be responsible for the weight loss of around 41% that occurred in the range of temperature between ambient temperature and 500 °C. Water loss is the cause of the endothermic reaction at T_{max} , DSC ~ 80 °C (broad T_{max} , DTG ~ 53 °C). The T_{max} , DSC ~ 170 °C (T_{max} , DTG ~ 180 °C) exothermic process is ascribed to the breakdown of anions NO_3^- (non-carbonized) and other nitrogen-containing compounds. A weight loss of around 14% along with an exothermic reaction around T_{max} , DSC ~ 250 °C (T_{max} , DTG ~ 240 °C) are probably caused by breakdown through oxidation of the gel network and also by the burning of the majority of the organic components. Weight reduced around 460 °C may be associated with the metal oxide phase formation of the perovskite BFO with loss of nearly ~ 3 % carbon trapped combustion to CO_2 gas (Table-1). BFO change its phase from (phase transition) from ferroelectric to paraelectric (T_c), which leads to the structural change, is responsible for the endothermic peak at 830 °C [36].

FT-IR spectral studies: The FT-IR spectra BFO powders calcinated at 400 °C and the precursor were acquired in the 4000-400 cm^{-1} range. Due to O-H stretching, broad absorption band in the 3500-3000 cm^{-1} region can be found which disap-

TABLE-1
STEPS FOR THERMAL DECOMPOSITION FOR $\text{Bi}(\text{NO}_3)_3 \cdot 5\text{H}_2\text{O}$ - $\text{Fe}(\text{NO}_3)_3 \cdot 9\text{H}_2\text{O}$ -PROPYLENE
GLYCOL PRECURSORS RECORDED WITH THE HEATING RATE OF 10°/min

Steps	Temperature range (°C)	Observed weight loss (%)	Species decomposed	T_{DSC} (°C)
I	25-150	14.12	H_2O	80 (endo)
II	150-200	10.21	NO_3^-	170 (exo)
III	200-300	14.37	Metal organic complexes	250 (exo)
IV	300-500	3.07	CO_2	460 (exo)

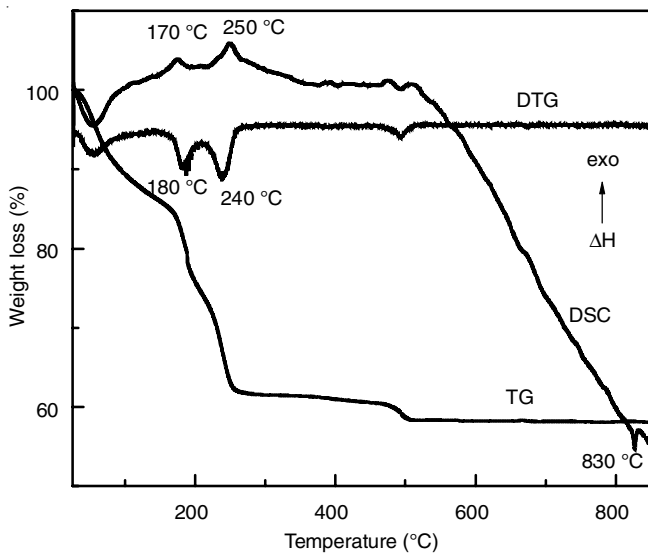


Fig. 1. TGA/DSC/DTG curves of the BFO powder precursor

peared when the temperature of the thermal treatment increases 400 °C [35,37]. Strong bands at ~1670 and ~1300 cm⁻¹ are attributed to C=O linkages that result from NO₃⁻ ions oxidizing propylene glycol's secondary C-OH group [35,38]. The strong bands at around 1590 for symmetric (ν_s) and 1350 cm⁻¹ for antisymmetric (ν_{as}) of the carboxylate (COO⁻) group, which are produced when the primary C-OH group of propylene glycol oxidizes [35,39]. Carboxylic groups produced here coordinated with the Fe(III) and Bi(III) cations to form carboxylate type complexes. In present study, the difference between ν_{as} and ν_s, which has a value of ~240 cm⁻¹, indicates that the carboxylate group formed above coordinates as monodentate (Fig. 2) [35,40].

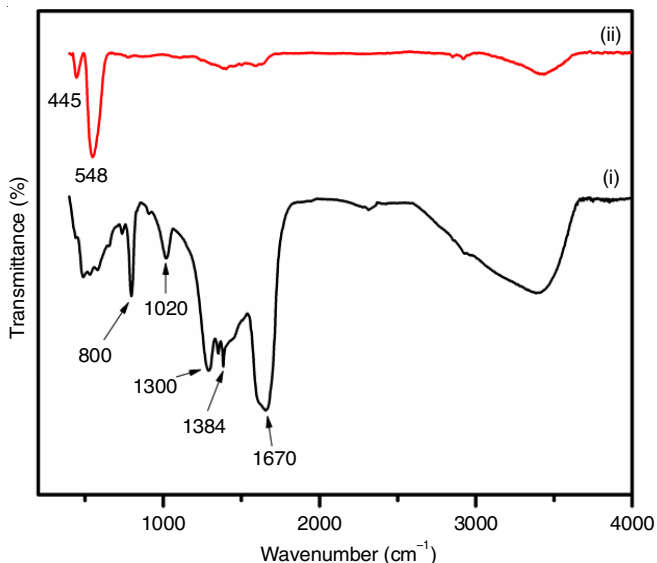


Fig. 2. FTIR spectra of BFO powder (i) precursor and (ii) calcined at 400 °C

The appearance of nitrate ions is responsible for the bands at approximately 1384, 1015 and 800 cm⁻¹ [28,38]. All of the organic peaks found in infrared range of the sample heated to 400 °C for 2 h vanish and two new absorption peaks of ~548

and ~445 cm⁻¹ are appeared. These peaks indicate the occurrence of Fe-O bond stretching and bending vibrations within the FeO₆ octahedra in the perovskite compounds [35,41].

XRD spectral studies: Fig. 3 shows the X-ray diffraction patterns of the precursor and BFO powder calcined at 400 °C for 2 h. After heat treatment, the BFO phase begins to form, fully developing at 400 °C, as evidenced by the appearance of intense diffraction peaks. The observed peaks in the XRD patterns can be indexed according to the powder diffraction data found on JCPDS card No. 86-1518. It shows that the diffraction peaks related to the BFO rhombohedral perovskite structure and the absence of distinctive peaks from any other phase suggests that phase pure BFO was formed *via* this pathway. The diffraction peaks of the calcined sample exhibit a significant line broadening indicates nanocrystalline nature of the synthesized BFO. The average crystallite size is estimated to be approximately 25 nm using the Scherrer's equation (eqn. 1), based on the (012), (104), (110), (202) and (024) peaks, after removing the instrumental contribution [42].

$$D = \frac{0.9\lambda}{\beta \cos \theta} \quad (1)$$

Here, D represents the average crystallite size, λ = 1.5406 is the X-ray wavelength and β is the corrected full width at half maximum (FWHM) of the diffraction peak at the diffraction angle 2θ.

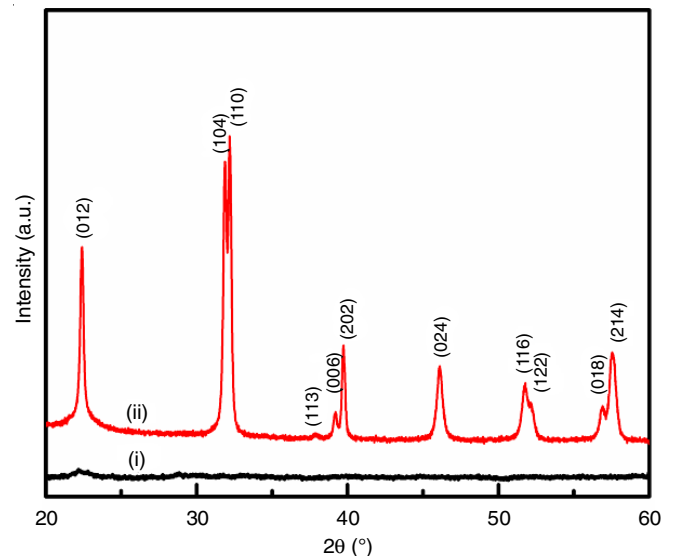


Fig. 3. XRD patterns of BFO powder (i) precursor and (ii) calcined at 400 °C

Morphological studies: Fig. 4 shows the TEM image of the perovskite-type BFO synthesized at 400 °C. In the process of synthesis, it has been established that the substance consists of nanoparticles. Moreover, the BFO particles show a uniform characteristic with size distribution ranging between 30 to 50 nm, which is much smaller than that of size distribution range of bulk BFO reported in the range of 1-3 μm and revealed that for the preparation of nanoscale BFO particles with uniform features sol-gel process is one of the best methods.

The XPS measurement at room temperature was performed to identify the composition, chemical and electronic state of

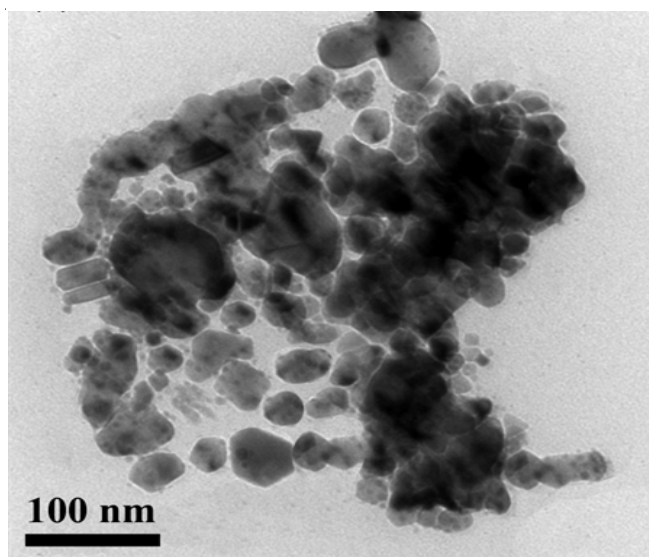


Fig. 4. TEM image for BFO nanoparticles prepared at 400 °C

an element. The XPS survey spectrum from 0 to 1000 eV is displayed in Fig. 5 for BFO nanoparticles synthesized at 400 °C, which indicates that when electrons are directly excited from core levels, a series of sharp peaks are observed. The prominent Bi 4f, Bi 4d and O 1s peaks, along with the less intense Bi 4p and Fe 2p peaks, confirmed the presence of Bi, Fe and O elements in the BFO nanoparticles. The spin-orbit doublet components of the Fe 2p photoemission, 2p_{3/2} and 2p_{1/2}, are detected at 710.8 eV and 724.2 eV, respectively [43]. These peaks are characteristic of Fe³⁺ and consistent with the literature data [44]. The spin-orbit doublet components of the Bi 4f photoemission, 4f_{7/2} and 4f_{5/2}, are observed at binding energies of 158.8 eV and 164.2 eV, respectively and these peaks belong to Bi³⁺ [45]. The XPS also confirmed that in the synthesized BFO, Bi and Fe are present as Bi³⁺ and Fe³⁺ valence state and it has a single phase agreement with the XRD results [43].

Raman spectral studies: Fig. 6 shows the Raman spectra at room temperature for the precursor and BFO powders calcined at 400 °C. According to group theory, 13 Raman-active modes ($\Gamma = 4A_1 + 9E$) are predicted for BFO, a perovskite with a rhombohedrally distorted structure and *R3c* space group [46].

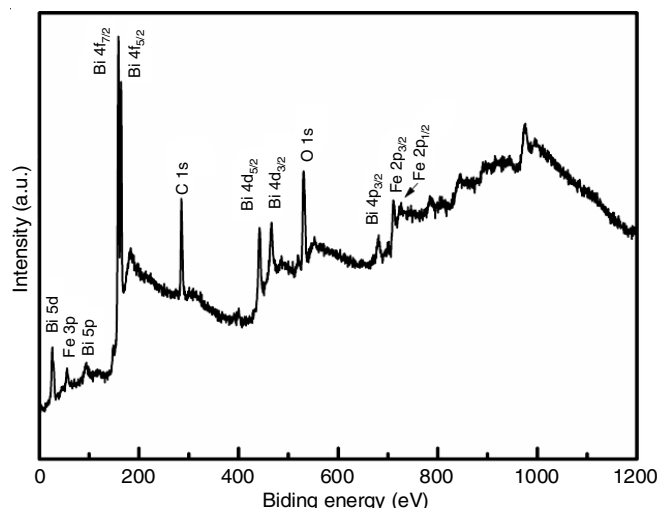


Fig. 5. XPS wide range spectrum analysis for BFO nanoparticles

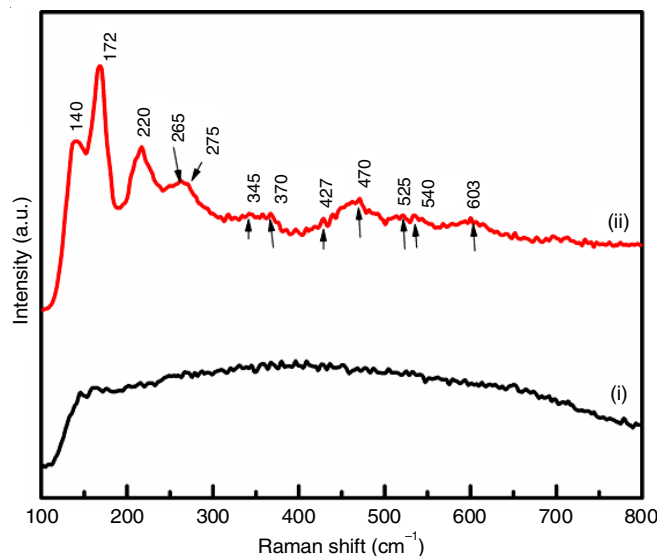


Fig. 6. Raman spectra of BFO powders at room temperature (i) precursor and (ii) calcined at 400 °C

In this study, eight transverse optical phonon modes with E-symmetry (E (TO)) and four transverse optical phonon modes with A₁-symmetry (A₁ (TO)) have been observed [43]. A peak

TABLE-2
COMPARISON OF THE RAMAN MODE POSITIONS (cm⁻¹) FROM PRESENT STUDY ON BFO NANOPARTICLES WITH REPORTED DATA ON SINGLE CRYSTALLINE BFO

Raman modes	Present study	Fukumura <i>et al.</i> [47]	Singh <i>et al.</i> [48]	Yuan <i>et al.</i> [49]	Mode assignments
A ₁ -1	140.2	147	136	136	Bi-O
A ₁ -2	172.4	176	168	168	Bi-O
A ₁ -3	220.3	227	212	211	Bi-O
A ₁ -4	427.0	490	425	425	Bi-O
E-1	–	77	72	–	Bi-O
E-2	265.4	260	–	–	Bi-O
E-3	275.5	279	275	275	Bi-O
E-4	345.6	351	335	335	Bi-O
E-5	370.2	375	363	365	Fe-O
E-6	470.3	437	–	456	Fe-O
E-7	525.0	473	456	–	Fe-O
E-8	540.8	525	549	549	Fe-O
E-9	603.4	598	597	597	Fe-O

at 427.0 cm⁻¹ with weak scattering intensity is classified as the A1-4 mode, while the three peaks with strong scattering intensities at 140.2, 172.4 and 220.3 cm⁻¹ are identified as the A1-1, A1-2 and A1-3 modes, respectively [35]. The next eight peaks with medium scattering intensities at 265.4, 275.5, 345.6, 370.2, 470.3, 525.0, 540.8 and 603.4 cm⁻¹ correspond to the E-2, E-3, E-4, E-5, E-6, E-7, E-8 and E-9 modes, respectively [35]. The Raman data (Table-2) observed for the polycrystalline BFO sample align well with previously reported single crystal BFO data by Fukumura *et al.* [47]. Similarly, it is consistent with the epitaxially grown BFO thin film data from Singh *et al.* [48] and BFO ceramic data from Yuan *et al.* [49] in terms of relative scattering intensity and mode frequency.

Optical properties of BFO nanoparticles: UV-vis DRS spectroscopy are used to investigate the optical characteristic of synthesized BFO NPs at room temperature and result are shown in Fig. 7. As the absorption cut-off wavelength is close to 600 nm, synthesized BFO nanoparticles may absorb visible light in the 400-600 nm range. This indicates that synthesized BFO NPs can absorb a significant quantity of visible light. To find the optical band-gap (E_g) of BFO NPs, the Tauc's formula is used which is given by, †

$$(\alpha h\nu)^2 = B(h\nu - E_g)$$

where α , h , ν , E_g and B stand for absorption coefficient, Planck constant, light frequency, band gap and a constant, respectively [50]. Fig. 7b displays the variation of $(\alpha h\nu)^2$ versus $(h\nu)$.

The linear part of the plot is fitted and the linear region is extrapolated on the energy axis, then the optical band gap was found to be 2.08 eV. Nguyen *et al.* [51] reported the band gap between 2.1-2.2 eV for the BFO nanoparticles synthesized by sonochemical method. Taazayet *et al.* [52] and Othman *et al.* [53] have observed the band gap 2.12 eV for the BFO nanoparticles synthesized by hydrothermal method. Nazeer *et al.* [18] found the band gap of 2.1 eV for the BFO nanoparticles synthesized by microemulsion route. The observed band gap of 2.08 eV in present work is consistent with these reports. The small band gap of 2.08 eV suggests that synthesized BFO

nanoparticles has potential application as visible or sunlight-mediated photocatalyst. It is anticipated that the synthesized BFO NPs with small crystallite size (based on XRD and TEM data) will have significant visible-light absorption capabilities towards efficient degradation of organic pollutants in the visible light range.

Conclusion

The sol-gel method using propylene glycol as complexing agent, successfully synthesizes pure BiFeO₃ nanocrystallites. The thermogravimetric analysis of as prepared BiFeO₃ precursor show the weight loss of ~ 41% between temperature range of room temperature and 550 °C is allocated to dehydration of the precursor, the decomposition of nitrate, the carbonization and volatilization of propylene glycol. The XRD analysis and Raman observation show that pure perovskite rhombohedral BiFeO₃ phase with *R3cis* synthesized after heat treatment at 400 °C for 2 h. The average crystallite size is get to be ~ 25 nm. The TEM studies show that all structure show nearly the spherical shape of particle constitutes the size range of 30-50 nm. The XPS spectra reveal that pure BiFeO₃ nanoparticles have single phase with Bi³⁺ and Fe³⁺ valence state. The optical band gap of BiFeO₃ is found to be 2.08 eV confirms that synthesized BiFeO₃ nanoparticles behave as efficient photocatalyst for the photocatalytic degradation of organic pollutants in the presence of sun light.

ACKNOWLEDGEMENTS

One of the authors, SKS, acknowledges University Grant Commission (UGC), New Delhi, India for providing BSR start-up grant to carry out this research work. All the authors are thankful to University Department of Chemistry, Lalit Narayan Mithila University of Darbhanga, Darbhanga, India for extending the laboratory facilities.

CONFLICT OF INTEREST

The authors declare that there is no conflict of interests regarding the publication of this article.

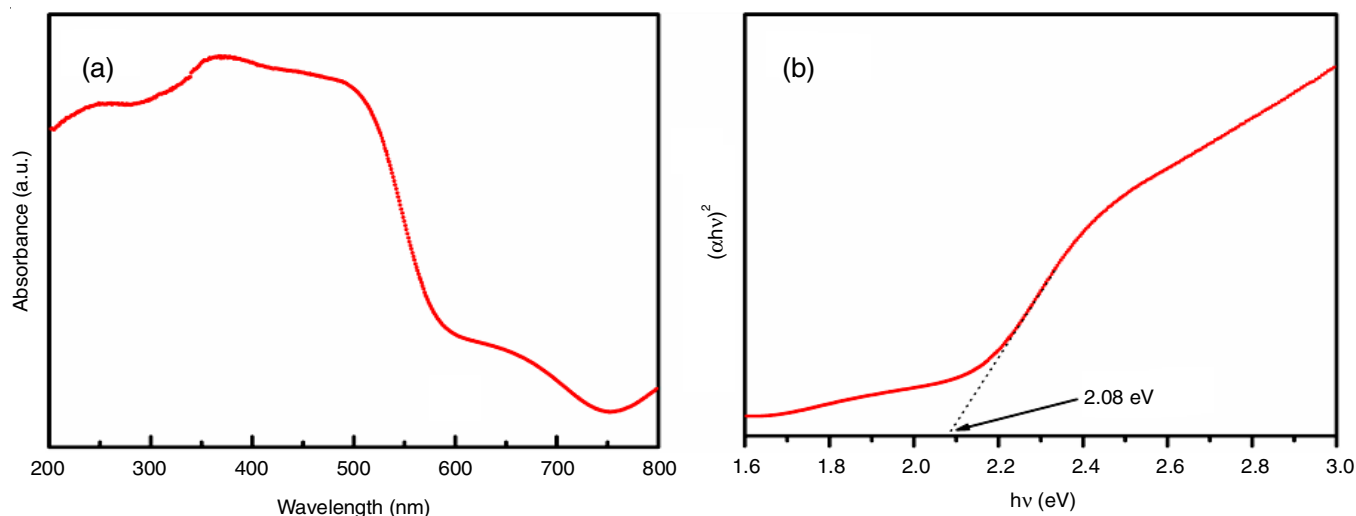


Fig. 7. (a) UV-visible spectrum of BFO nanoparticles calcined at 400 °C; (b) corresponding plot of $(\alpha h\nu)^2$ vs. photon energy for the BFO nanoparticles

REFERENCES

- A.M. Awad, S.M.R. Shaikh, R. Jalab, M.H. Gulied, M.S. Nasser, A. Benamor and S. Adham, *Sep. Purif. Technol.*, **228**, 115719 (2019); <https://doi.org/10.1016/j.seppur.2019.115719>
- A.M. Awad, R. Jalab, A. Benamor, M.S. Nasser, M.M. Ba-Abbad, M. El-Naas and A.W. Mohammad, *J. Mol. Liq.*, **301**, 112335 (2020); <https://doi.org/10.1016/j.molliq.2019.112335>
- H. Lu, J. Wang, M. Stoller, T. Wang, Y. Bao and H. Hao, *Adv. Mater. Sci. Eng.*, **2016**, 4964828 (2016); <https://doi.org/10.1155/2016/4964828>
- Z. Li, G. Wang, K. Zhai, C. He, Q. Li and P. Guo, *Colloids Surf. A Physicochem. Eng. Asp.*, **538**, 28 (2018); <https://doi.org/10.1016/j.colsurfa.2017.10.046>
- H. Shirzadi and A. Nezamzadeh-Ejehieh, *J. Mol. Liq.*, **230**, 221 (2017); <https://doi.org/10.1016/j.molliq.2017.01.029>
- K. Hashimoto, H. Irie and A. Fujishima, *Jpn. J. Appl. Phys.*, **44(12R)**, 8269 (2005); <https://doi.org/10.1143/JJAP.44.8269>
- J. Schneider, M. Matsuoka, M. Takeuchi, J. Zhang, Y. Horiuchi, M. Anpo and D.W. Bahnemann, *Chem. Rev.*, **114**, 9919 (2014); <https://doi.org/10.1021/cr50001892>
- K. Qi, B. Cheng, J. Yu and W. Ho, *J. Alloys Compd.*, **727**, 792 (2017); <https://doi.org/10.1016/j.jallcom.2017.08.142>
- Y. Lv, J. Lin, S. Peng, L. Zhang and L. Yu, *New J. Chem.*, **43**, 19223 (2019); <https://doi.org/10.1039/C9NJ04767K>
- G.-J. Lee and J.J. Wu, *Powder Technol.*, **318**, 8 (2017); <https://doi.org/10.1016/j.powtec.2017.05.022>
- J.-C. Sin, S.-M. Lam, A.R. Mohamed and K.-T. Lee, *Int. J. Photoenergy*, **2012**, 185159 (2012); <https://doi.org/10.1155/2012/185159>
- M. Ge, C. Cao, J. Huang, S. Li, Z. Chen, K.-Q. Zhang, S.S. Al-Deyab and Y. Lai, *J. Mater. Chem. A Mater. Energy Sustain.*, **4**, 6772 (2016); <https://doi.org/10.1039/C5TA09323F>
- L. Yin and W. Mi, *Nanoscale*, **12**, 477 (2020); <https://doi.org/10.1039/C9NR08800H>
- S. Irfan, Z. Zhuanghao, F. Li, Y.-X. Chen, G.-X. Liang, J.-T. Luo and F. Ping, *J. Mater. Res. Technol.*, **8**, 6375 (2019); <https://doi.org/10.1016/j.jmrt.2019.10.004>
- M. Pooladi, I. Sharifi and M. Behzadipour, *Ceram. Int.*, **46**, 18453 (2020); <https://doi.org/10.1016/j.ceramint.2020.04.241>
- S.-M. Lam, J.-C. Sin and A.R. Mohamed, *Mater. Res. Bull.*, **90**, 15 (2017); <https://doi.org/10.1016/j.materresbull.2016.12.052>
- A. Haruna, I. Abdulkadir and S.O. Idris, *Heliyon*, **6**, e03237 (2020); <https://doi.org/10.1016/j.heliyon.2020.e03237>
- Z. Nazeer, I. Bibi, F. Majid, S. Kamal, N. Alwadai, M.I. Arshad, A. Ali, S. Nouren, M. Al Huwayz and M. Iqbal, *ACS Omega*, **9**, 545 (2024); <https://doi.org/10.1021/acsomega.3c06132>
- C. Ponraj, C. Krishnamoorthi, G. Vinita, N. Manikandan, P. Santhosh kumar and J. Daniel, *ChemistrySelect*, **8**, e202301180 (2023); <https://doi.org/10.1002/slct.202301180>
- C. Michel, J.-M. Moreau, G.D. Achenbach, R. Gerson and W.J. James, *Solid State Commun.*, **7**, 701 (1969); [https://doi.org/10.1016/0038-1098\(69\)90597-3](https://doi.org/10.1016/0038-1098(69)90597-3)
- P. Fischer, M. Polomska, I. Sosnowska and M. Szymanski, *J. Phys. Chem.*, **13**, 1931 (1980); <https://doi.org/10.1088/0022-3719/13/10/012>
- W. Eerenstein, N. Mathur and J. Scott, *Nature*, **442**, 759 (2006); <https://doi.org/10.1038/nature05023>
- G. Catalan and J.F. Scott, *Adv. Mater.*, **21**, 2463 (2009); <https://doi.org/10.1002/adma.200802849>
- R. Palai, R.S. Katiyar, H. Schmid, P. Tissot, S. Clark, J. Robertson, S. Redfern, G. Catalan and J. Scott, *Phys. Rev. B Condens. Matter Mater. Phys.*, **77**, 014110 (2008); <https://doi.org/10.1103/PhysRevB.77.014110>
- J. Silva, A. Reyes, H. Esparza, H. Camacho and L. Fuentes, *Integr. Ferroelectr.*, **126**, 47 (2011); <https://doi.org/10.1080/10584587.2011.574986>
- Q. Zhang, D. Sando and V. Nagarajan, *J. Mater. Chem. C Mater. Opt. Electron. Devices*, **4**, 4092 (2016); <https://doi.org/10.1039/C6TC00243A>
- T. Liu, Y. Xu and J. Zhao, *J. Am. Ceram. Soc.*, **93**, 3637 (2010); <https://doi.org/10.1111/j.1551-2916.2010.03945.x>
- T. Liu, Y. Xu, S. Feng and J. Zhao, *J. Am. Ceram. Soc.*, **94**, 3060 (2011); <https://doi.org/10.1111/j.1551-2916.2011.04536.x>
- S.-Z. Lu and X. Qi, *J. Am. Ceram. Soc.*, **97**, 2185 (2014); <https://doi.org/10.1111/jace.12960>
- S. Ghosh, S. Dasgupta, A. Sen and H.S. Maiti, *J. Am. Ceram. Soc.*, **88**, 1349 (2005); <https://doi.org/10.1111/j.1551-2916.2005.00306.x>
- S.M. Selbach, M.-A. Einarsrud, T. Tybell and T. Grande, *J. Am. Ceram. Soc.*, **90**, 3430 (2007); <https://doi.org/10.1111/j.1551-2916.2007.01937.x>
- Q.-H. Jiang, C.-W. Nan and Z.-J. Shen, *J. Am. Ceram. Soc.*, **89**, 2123 (2006); <https://doi.org/10.1111/j.1551-2916.2006.01062.x>
- M. Popa, D. Crespo, J. Calderon-Moreno, S. Preda and V. Fruth, *J. Am. Ceram. Soc.*, **90**, 2723 (2007); <https://doi.org/10.1111/j.1551-2916.2007.01779.x>
- J. Wei and D. Xue, *Mater. Res. Bull.*, **43**, 3368 (2008); <https://doi.org/10.1016/j.materresbull.2008.02.009>
- S.K. Srivastav and N.S. Gajbhiye, *J. Am. Ceram. Soc.*, **95**, 3678 (2012); <https://doi.org/10.1111/j.1551-2916.2012.05411.x>
- J.K. Kim, S.S. Kim and W.-J. Kim, *Mater. Lett.*, **59**, 4006 (2005); <https://doi.org/10.1016/j.matlet.2005.07.050>
- A.C. Tas, P. Majewski and F. Aldinger, *J. Am. Ceram. Soc.*, **83**, 2954 (2000); <https://doi.org/10.1111/j.1151-2916.2000.tb01666.x>
- M. Stoia, P. Barvinschi, L.B. Tudoran, M. Barbu and M. Stefanescu, *J. Therm. Anal. Calorim.*, **108**, 1033 (2011); <https://doi.org/10.1007/s10973-011-1903-0>
- R. Prasad, A. Sulaxna and A. Kumar, *J. Therm. Anal. Calorim.*, **81**, 441 (2005); <https://doi.org/10.1007/s10973-005-0804-5>
- V. Zelenik, Z. Vargovi and K. Györyovi, *Spectrochim. Acta A Mol. Biomol. Spectrosc.*, **66**, 262 (2007); <https://doi.org/10.1016/j.saa.2006.02.050>
- G.V.S. Rao, C.N.R. Rao and J.R. Ferraro, *Appl. Spectrosc.*, **24**, 436 (1970); <https://doi.org/10.1366/000370270774371426>
- B.D. Cullity, *Elements of X-ray Diffractions*, Addison-Wesley, USA, (1978).
- S.K. Srivastav, N.S. Gajbhiye and A. Banerjee, *J. Appl. Phys.*, **113**, 203917 (2013); <https://doi.org/10.1063/1.4807928>
- K. Wandelt, *Surf. Sci. Rep.*, **2**, 1 (1982); [https://doi.org/10.1016/0167-5729\(82\)90003-6](https://doi.org/10.1016/0167-5729(82)90003-6)
- X. Zhu, Q. Hang, Z. Xing, Y. Yang, J. Zhu, Z. Liu, N. Ming, P. Zhou, Y. Song, Z. Li, T. Yu and Z. Zou, *J. Am. Ceram. Soc.*, **94**, 2688 (2011); <https://doi.org/10.1111/j.1551-2916.2011.04430.x>
- R. Haumont, J. Kreisel, P. Bouvier and F. Hippert, *Phys. Rev. B Condens. Matter Mater. Phys.*, **73**, 132101 (2006); <https://doi.org/10.1103/PhysRevB.73.132101>
- H. Fukumura, H. Harima, K. Kisoda, M. Tamada, Y. Noguchi and M. Miyayama, *J. Magn. Magn. Mater.*, **310**, e367 (2007); <https://doi.org/10.1016/j.jmmm.2006.10.282>
- M.K. Singh, H.M. Jang, S. Ryu and M.-H. Jo, *Appl. Phys. Lett.*, **88**, 042907 (2006); <https://doi.org/10.1063/1.2168038>
- G.L. Yuan, S.W. Or and H.L.W. Chan, *J. Appl. Phys.*, **101**, 064101 (2007); <https://doi.org/10.1063/1.2433709>
- J. Tauc, R. Grigorovici and A. Vancu, *Phys. Status Solidi, B Basic Res.*, **15**, 627 (1966); <https://doi.org/10.1002/pssb.19660150224>
- H.P. Nguyen, G. Gyawali, Y.H. Jo, T.-H. Kim and S.W. Lee, *Res. Chem. Intermed.*, **43**, 5113 (2017); <https://doi.org/10.1007/s11164-017-3047-8>
- W. Ben Tazayet, I. Mallek Zouari, P. Gemeiner, B. Dkhil and N. Thabet Mliki, *Rapid Res. Letts.*, **16**, 2200081 (2022); <https://doi.org/10.1002/pssr.202200081>
- M. Othman, I. Mallek-Zouari, H. Akrouit and N.T. Mliki, *Ceram. Int.*, **49**, 10580 (2023); <https://doi.org/10.1016/j.ceramint.2022.11.245>